Manufacturing and Testing of a Sandwich panel honeycomb core reinforced with natural-fiber fabrics

Ariel Stocchi, Lucas Colabella, Adrián Cisilino, Vera Álvarez

PII: S0261-3069(13)00906-0
DOI: http://dx.doi.org/10.1016/j.matdes.2013.09.054
Reference: JMAD 5885

To appear in: *Materials and Design*

Received Date: 4 July 2013
Accepted Date: 7 September 2013

Please cite this article as: Stocchi, A., Colabella, L., Cisilino, A., Álvarez, V., Manufacturing and Testing of a Sandwich panel honeycomb core reinforced with natural-fiber fabrics, *Materials and Design* (2013), doi: http://dx.doi.org/10.1016/j.matdes.2013.09.054

Manufacturing and Testing of a Sandwich panel honeycomb core reinforced with natural-fiber fabrics

Ariel Stocchi[1]*,Lucas Colabella[2], Adrián Cisilino[2] and Vera Álvarez[1]

[1]Composite Materials (CoMP) and [2]Mechanics of Materials group, Materials Science and Technology Research Institute (INTEMA), University of Mar del Plata – CONICET.

Av. Juan B. Justo 4302 - B7608FDQ - Mar del Plata, ARGENTINA

Telephone +54 223 4816600

*To whom correspondence should be addressed. E-Mail: arstocchi@fi.mdp.edu.ar

Abstract

A novel honeycomb core made of a natural-fiber reinforced composite consisting of a vinylester matrix reinforced with jute fabric is introduced. Six-mm- and 10-mm-cell honeycombs are manufactured using two compression-molding techniques. Best results are obtained for the mold with lateral compression. Experimental tests are conducted to characterize the elastic response of the composite and the core response under flatwise compression. The effective elastic properties of the core are computed via a homogenization analysis and finite element modeling. The results of the homogenization analysis are in very good agreement with estimations done using analytical formulas from the bibliography. The flatwise compression tests show that the core failure mechanisms are yarn pull-out and fiber breaking. The large wall thickness relative to the cell size of the jute-vinylester cores, which inhibits buckling, and the heterogeneities in the composite, which are preferential damage initiation sites, explain the observed behavior. When compared in terms of the specific strengths, the jute/vinylester cores introduced in this work show similar performances to those of their commercially available counterparts. The results from this study suggest that jute-reinforced cores have the potential to be an alternative to standard cores in applications that sustain compressive static loads.

Keywords: honeycomb cores; natural fibers; mechanical characterization; effective elastic properties.

1. Introduction

Sandwich panels are widely used as a means to build high-performance lightweight structures [1, 2]. Sandwich panels consist of two thin and stiff face-sheets (or skins) bonded to a thick and light core. The face sheets provide the flexural stiffness and strength to the panel, while the role of the core is to transmit the shear between the face sheets. A strong core can also contribute to the flexural stiffness and to the out-of-plane shear and compressive strength of the panel [1, 3]. On the other hand, a core with poor mechanical properties undermines the performance of the panel [3]. Typically, cores are made of foams or balsa [4, 5] or they are fabricated using corrugated, truss or honeycomb structures [6, 7]. Corrugated cores provide unidirectional support to the skins [8, 9], while honeycomb cores provide bidirectional support [1]. The most used materials in honeycomb fabrication are aluminum, polymers and composites like Nomex [10].

Sandwich panels are used not only because of their advantages in terms of weight saving and structural performance, but also as an effective means to reduce costs [11]. Thus, there is always an interest in the development of new materials and designs for low-cost high-performance cores. In particular, the large cell-size of the sandwich structures for civil applications (typically in the range from 500 mm to 1500 mm) allows the fabrication of cores using fiber-reinforced polymers [12]. For example, Ji et al [12] introduced a glass-fiber reinforced-polymer corrugated-core which is fabricated via the assembly of pultruded and thermoformed shapes [13].

At the same time, there is also an increasing interest to substitute glass and carbon fibers by natural ones [14]. Natural fibers present some advantages when compared to their synthetic counterparts: they are cheaper, they have lower mass per unit area, they are eco-friendly, recyclable and biodegradable by nature, they do not

produce skin irritation, and they provide good acoustic-insulating properties [15-17]. In contrast, natural-fiber reinforced composites have substantially inferior mechanical performance and water resistance properties than conventional glass-fiber reinforced composites [18, 19]. In any case, natural-fiber reinforced materials have found uses in several novel applications, ranging from furniture and packaging to more complex engineering uses, such as building materials and structural parts for automobiles [20-22].

There are developments towards the use natural fibers for the reinforcement of sandwich-panels cores. In this sense, Rao et al. [23, 24] have introduced hollow cores made of polypropylene with chopped sisal fibers as reinforcement. These cores are fabricated using thermoforming and assembling process. Thin continuous rolls of the sisal–polypropylene composite are produced in conical twin screw extruders and then thermoformed into half hexagonal or sinusoidal profiles. Finally, the profiles are attached together by ultrasonic bonding. Rao et al. [23, 24] conclude that their panels are suitable in automobile, aerospace, packaging and building/construction industries. Recently, Petrone et al. have studied polymeric honeycombs reinforced with short and continuous flax fibers. They report results about the impact and dynamic behaviors of the panels [25] and about the feasibility to use them in structural and functional applications [26] .

It is introduced in this paper a novel honeycomb core made of a natural-fiber reinforced composite. The composite consists of a thermoset-polymer (vinylester) reinforced with jute fabrics. The paper reports the details of two methods for the fabrication of 6-mm and 10-mm cell-size cores, the experimental characterization of the anisotropic elastic behavior of the composite, and the experimental characterization of the core response under flatwise compression. The failure

mechanisms of the core in the compression tests are identified and discussed. In addition, there are also reported the effective elastic properties of the 10-mm cell core, which are computed via a computational homogenization method. The specific strengths of the cores are compared to those of commercially available products.

2. Materials and experimental methods

2.1 Honeycomb fabrication

The matrix material was prepared using the general-purpose vinylester resin Derakane Momentum 411-350 (Dow Chemical) provided by Poliresinas San Luis (Argentina). Methyl ethyl ketone peroxide (MEKP) was used as catalyst in a weight ratio of 1:0.05. The reinforcement material was a commercially available woven jute fabric provided by Casthanal Textil CIA (Brazil). The fabric surface density was around 300 g/m^2 and the average yarn diameter of the jute was 0.9 mm. The jute fabrics were washed with distilled water and detergent solution, and then dried to constant weight in a vacuum oven at 80 ºC.

The honeycomb cores were manufactured by compression molding at laboratory scale using two molds:

a) *Mold with fixed inserts*. The walls and the inserts with the shape of the cells were kept in place by screwing them to the bottom plate from behind, see Figure 1. The mold dimensions were 120 mm in length (ribbon direction), 30 mm in width and 10 mm in height, and it contained a 5×18 array of 6-mm (cell size) hexagonal inserts. The clearance between the inserts, and thus the honeycomb wall thickness, was t= 1.4 mm.

To prepare the fiber-reinforced honeycombs, the jute fabric was placed between the inserts following a zigzag pattern in the ribbon direction. In order to facilitate the

placement of the reinforcement and its uniform distribution along the walls, the jute fabric was put in place at the same time the inserts were fixed to the bottom plate. No longitudinal force was applied to the jute fabric while disposing it into the mold. Afterwards, the vinylester was poured into the mold at 20℃. Then, the ensemble was molded under a 50-MPa pressure in a hydraulic press during 1 h at 80 ºC. Finally, the cores were post cured during 2 h at 140 ºC in an oven. The wall thickness resulted in t=1.43 ± 0.10 mm. It is worth to note that as consequence of the manufacturing process, the average fiber-volume contents are different for the longitudinal and diagonal walls. Since the longitudinal walls contain two fabric-layers, its fiber content should double that of the diagonal walls, which have a single fabric layer. This was confirmed by the experimental measurements, which resulted in fiber volume contents of 29% and 14% for the longitudinal and the diagonal walls, respectively. A picture of the honeycomb core is shown in Figure 2.

Although effective, this fabrication method has a drawback due to the fixed position of the inserts: it is not possible to press the walls in the direction of the thickness during the curing process. This limitation undermines optimum consolidation of the fibers into the cell wall. A second manufacturing method is proposed next to walk around these problems.

b) *Lateral compression mold*. The second mold allowed for the lateral compression of the ensemble. It consisted in a series of aluminum “combs” with the shape of the cells, which could displace laterally, see Figure 3. This mold was used to manufacture samples of size 120 mm×60 mm×10 mm with a 12×6 cell array. In order to improve ease of manipulation the cell size was changed to 10mm.

To fabricate the honeycombs, the resin-wetted jute fabrics were intercalated between the combs in the ribbon direction. As in the previous method, no

longitudinal force was applied to the jute fabric while disposing it into the mold. Then, the ensemble was laterally pressed and clamped to remove the excess of resin and to drag entrapped air bubbles. The process was completed with the thermal treatments to cure and post-cure the resin, like in the previous method.

A picture of the honeycomb is depicted in Figure 4. When compared to the previous manufacturing method, the wall thickness diminished to t=1.11 ± 0.10 mm. The fiber volume contents augmented accordingly to 40% and 20% for the longitudinal and the diagonal walls, respectively.

In addition to the honeycombs, there were also manufactured plane sheets of the jute-vinylester composites to prepare samples for the mechanical characterization of the wall materials. Thus, there were prepared sheets containing one and two fabric layers, as in the longitudinal and diagonal walls. Special care was taken to replicate the manufacturing conditions of the honeycomb in order to obtain samples with the same thicknesses and fiber contents.

3. Experimental characterization

3.1 Core characterization

The mechanical characterization of the honeycombs comprised the tests to evaluate the flatwise compression strength and flexural modulus. Compression (crushing) tests were practiced on both cores according to the ASTM: C365/C365M standard using an Instron 4467 machine. The test speed was 0.5 mm/min and the sample dimensions were 55 mm×22 mm×10 mm. A set with 6 samples was tested in each case.

The flexural modulus of the cores was measured for the 10 mm-cell core only. The test was performed according to the ASTM: D790, with crosshead speed of 1.5

mm/min and a span *S*=70 mm. Six specimens with length *L*=80 mm (ribbon direction), width *W*=36 mm and height *H*=10 mm were tested and their flexural moduli, E_{flex}, computed using Eq (1),

$$E_{flex} = \frac{S^3 m}{4WH^3} \quad (1)$$

where m is the slope of the linear portion of the load-displacement record.

Failure mechanisms resulting from the compression tests were studied by means of Scanning Electron Microscopy (SEM) observations. Samples were gold-plated using standard procedures.

In order to compare the performances of the honeycombs in terms of their specific mechanical properties, the specimens were weighted and their densities computed. The density results and geometrical data of the honeycombs are listed in Table 1 (see Figure 5a for the identification of the geometrical parameters). There are also given in Table 1 the data of commercially available honeycombs, which will be used later for comparison.

4. Results and discussion

4.1 Honeycomb cores mechanical response

The stress–strain curves of the two jute-vinylester honeycombs are plot in Figure 6. There are also plot in Figure 6 the stress–strain response curves of Nomex and aluminum cores [27, 28] in order to show the typical compression behavior of honeycomb structures. The compression behavior of honeycombs allows identifying three distinct stages. In the first stage the stress rises linearly until a peak load is reached. After this point, there is a sudden drop of the curve due to the buckling of the cell walls. This is the starting point for the second stage, in which the folding of

the cells develops under an almost constant load. In the case of aluminum honeycombs, the walls deform plastically while folding. On the other hand, the folding of the Nomex, which is relatively brittle compared to aluminum, results in fractures in the cell walls. In both cases, the amount of folding increases and eventually extends over the entire height of the cells. The third stage is usually referred as the "densification" stage, and it results in the rapid increment in the stress due to the contact between the cell walls.

It can be observed from Figure 6, that the cores produced in this work do not exhibit the abrupt stress drop between the initial linear behavior and the stress plateau. In contrast, they present a gradual transition between these two stages. The 10-mm-cell core attains the stress plateau at 55% strain while the 6-mm-cell one does at 35% strain. At the same time, the jute-vinylester cores possess relatively high compression strengths when compared to the commercially available cores: σ_c = 15.5 MPa for the 6-mm-cell core and σ_c= 13.5 MPa for the 10-mm-cell one (see Table 1).

The characteristic behavior of the honeycombs produced in this work is consequence of their failure mechanisms. In contrast to the Nomex and aluminum cores described above, the jute-vinylester cores do not suffer of the unstable failure due to buckling of the cell walls, but a progressive damage due to typical fiber-composite failure mechanisms: yarn pull-out, fiber breaking and axial splitting. These failure mechanisms are shown in Figures 7 and 8. In particular, the micrograph in Figure 8a shows a typical yarn pull-out, while the closed-up in Figure 8b allows observing the fiber breakage and axial splitting. Figure 8b also shows the plastic deformation in the matrix. The cell geometry and the heterogeneous nature of the material can explain this behavior. On one hand, the relative high aspect ratio

between the wall thickness to the cell size (see from Table 1 that t/c =0.24 and 0.11 for the 6-mm-cell and the 10-mm-cell cores, respectively, in contrast to $0.016 \leq t/c \leq 0.047$ for the commercially available cores) results in higher critical buckling loads. On the other hand, it can be argued that the heterogeneities in the jute-vinylester composite due to local variations in the fiber properties and orientation are preferential damage initiation sites. Thus, the damage of the composite starts before the critical buckling load is attained. It is worth to note that this behavior has been also observed in Nomex cores. There is evidence in the bibliography showing that the failure mode can switch from buckling to fracture for high density Nomex cores [29].

Finally, the performance of the cores is compared in terms of their specific compression strengths. It is interesting to see from Table 1, that even when it presents a compression strength lower than the 6-mm-cell core, the 10-mm-cell jute-vinylester honeycomb results in the best performance due to its lower density. The specific compression strength for the 10-mm- and the 6-mm-cores are σ_{cs} =0.085 MPa/Kg and σ_{cs} =0.051 MPa/Kg, respectively. These results are compared in Figure 9 to the specific compression strengths of the commercially available cores listed in Table 1. It can be observed that the cores produced in this work have a performance comparable to those of the commercially available products. Moreover, the 10-mm-cell jute-vinylester core has superior specific compression performance than any of the listed cores.

The resulting value for the flexural modulus of the 10-mm-cell jute-vinylester core was E_{flex} =115.48 ± 1.35 MPa. It is observed that the dispersion of E_{flex} is relatively high, around 40% the mean value. This dispersion is attributed to the heterogeneity

and dispersion of the properties of the jute reinforcement. This result will be used later for the validation of the finite element models.

4.2 Elastic characterization of the composite

The elastic properties of the composite were appraised by means of uniaxial tensile tests monitored with Digital Image Correlation (DIC) strain measurements. Tensile tests were performed according to the ASTM: D3518/D3518M to obtain the Young Modulus and the Poisson's Ratio, and ASTM: D3039/D3039M to obtain the Shear Modulus. All tests were carried out using an Instron 4467 machine. The test speed was 1 mm/min. The specimen geometry and dimensions are depicted in Figure 10. Specimens were laser-cut from the jute-vinylester sheets using two orientations: with their transversal and longitudinal directions, (i_1,i_2), coincident and rotated 45º with the fabric orthotropic directions (e_1,e_2), see Figures 10a and 10b, respectively. Three specimens were tested for each orientation, for both, the composites with one and two fabric layers.

DIC was chosen due to its ability to measure the complete displacement field, what it is especially suitable to characterize the anisotropic elastic response of the composites. DIC measurements were carried out using an in-house developed set-up based on a Canon EOS Rebel XSI 12.2 Megapixel digital camera commanded via a computer. The data processing was made using the software *Digital Image Correlation and Tracking* due to Eberl and available at Matlab Central [30]. This software uses the zero-normalized cross-correlation criterion [31] and reaches a sub-pixel resolution using peak-finding algorithm [32]. The software capabilities were extended to compute the strains via the differentiation of the displacement field using a point wise least squares algorithm [33].

The DIC experimental setup was calibrated and validated via a set of tests. Synthetic computer-generated distortion patterns were used to assess the performance of the algorithms in the absence of experimental artifacts. Besides, measurements performed on specimens made of expanded polystyrene, ethyl-vinyl-acetate and polymethyl-methacrylate, and instrumented with a mechanical extensometer were used to devise and calibrate the methods for the specimen preparation, camera alignment and to account for the camera-lens optical aberrations. The preparation of specimen surface consisted in the deposition of a fine black spray over a matte-white coating. This resulted in a random speckle pattern like that illustrated in Figure 11a. The overall measurement error of the DIC was estimated less than 2%.

The composite in-plane elastic constants were computed using the load and strain fields measured in the tensile tests. As an example, Figure 12 depicts the stress vs strain plots resulting from three tensile specimens for the composite with two-fabric-layers and the load oriented 45º with respect to the fabric orthotropic directions. Figure 11b shows the corresponding strain fields calculated by DIC for the stress level σ= 12 MPa. The scatter of the DIC results in Figure 11b is consequence of the presence of the fibers, and the local variations in their spatial distribution and orientation (see Figure 10).

The resulting in-plane elastic properties of the composites are reported in Table 2. As it was expected, the Young modulus of the two-fabric-layer composite nearly doubles that of the one-fabric-layer one, while Poisson ratios and the shear moduli are practically the same for both composites. Assuming an orthotropic symmetry, the stiffness tensors for the one- and two-fabric layer composites expressed in the (e_1, e_2, e_3) system are computed using standard procedures [34]:

$$C_1 = \begin{bmatrix} 4666 & 1593 & 1577 & 0 & 0 & 0 \\ 1593 & 4666 & 1577 & 0 & 0 & 0 \\ 1577 & 1577 & 3994 & 0 & 0 & 0 \\ 0 & 0 & 0 & 1231 & 0 & 0 \\ 0 & 0 & 0 & 0 & 1231 & 0 \\ 0 & 0 & 0 & 0 & 0 & 1240 \end{bmatrix} [MPa] \quad (2)$$

and

$$C_2 = \begin{bmatrix} 8549 & 2635 & 1451 & 0 & 0 & 0 \\ 2635 & 8549 & 1451 & 0 & 0 & 0 \\ 1451 & 1451 & 3580 & 0 & 0 & 0 \\ 0 & 0 & 0 & 1231 & 0 & 0 \\ 0 & 0 & 0 & 0 & 1231 & 0 \\ 0 & 0 & 0 & 0 & 0 & 1211 \end{bmatrix} [MPa], \quad (3)$$

respectively.

It is worth to mention that due to impossibility of performing tests in the direction of the sheet thickness, the elastic properties in the e_3 -directions were assumed equal to those of the neat isotropic vinylester matrix, $E_{33} = E_M = 3200$ [MPa] and $v_{13} = v_m = 0.3$.

4.3 Effective elastic properties

Homogenization with periodic boundary conditions [35] was used to estimate the effective elastic properties of the 10-mm-cell core. The use of periodic boundary conditions was chosen because it provides the closest agreement with the actual material behavior [36].

Following the standard finite element approach, a set of six linear-independent boundary value problems with periodic boundary conditions was solved for the core unit cell. The software Abaqus 6.10 [34] was used for the finite element analyses. The model for the unit cell was discretized using regular mesh of quadratic hexahedral elements (C3D8R), see Figure 13a. The black elements are in the solid portion of the unit cell, while the gray ones correspond to the void portion. The

elastic properties of the solid part were specified as C_1 or C_2 (see equations (2) and (3)), whether they corresponded to the one or two fabric-layer material, respectively. Besides, relatively pliant elastic properties, E_{void} = 10^{-5} MPa and ν_{void} =0 were assigned to the elements in the void part. The periodic boundary conditions were specified via the *EQUATION command using the strategy proposed by Barbero [37]. As an example, Figure 13b illustrates the periodic deformation for the unit cell model for the in-plane shear load case. The effective elastic properties for the core were computed from the finite element results using the homogenization method via an in-house developed Matlab function [36]. The accuracy of the implementation was verified by comparison of results for some benchmark problems reported by Guedes and Kikuchi [38]. There was also carried out a convergence analysis to assess the effects of the mesh size, and it was found that a regular discretization of 98×56×19 elements provides mesh independent results.

The homogenization analysis resulted in the following effective stiffness tensor for the 10-mm-cell core:

$$C_{eff} = \begin{bmatrix} 333 & 275 & 168 & 0 & 0 & 0 \\ 275 & 316 & 162 & 0 & 0 & 0 \\ 168 & 162 & 1316 & 0 & 0 & 0 \\ 0 & 0 & 0 & 31 & 0 & 0 \\ 0 & 0 & 0 & 0 & 170 & 0 \\ 0 & 0 & 0 & 0 & 0 & 174 \end{bmatrix} [MPa]. \quad (4)$$

The result in Eq.(4) is expressed in the core reference system (x, y, z), see Figures 5(a) and 13. Furthermore, the effective engineering elastic constants were computed from C_{eff} using standard procedures [34]: E_{xx} =93.09 MPa, E_{yy} =88.46 MPa, E_{zz} =1225 MPa, G_{xy} =31 MPa, G_{xz} =170 MPa and G_{yz} =174 MPa.

The above results were verified by comparison to analytical formulae from the bibliography. It is worth to note that in every case, the analytical solutions from the

bibliography were checked for its applicability to the present case. Particular care was taken in what respected to the hypotheses about the thickness and behavior of the diagonal walls when compared to those of the longitudinal ones.

The formulae due to Gibson and Ashby [39] was used to compute the in-plane equivalent Young moduli E^*_{xx} and E^*_{yy}. These formulae reduce the in-plane rigidity of honeycombs to depend on the elasticity and the dimensions of the diagonal walls only. In particular, for regular hexagonal cores, $E^*_{xx} = E^*_{yy}$ is estimated using the following equation:

$$E^*_{xx} = E^*_{yy} = 2.3\left(\frac{t}{l}\right)^3 E^d_{11} = 60.62\,MPa \tag{5}$$

where l = 5.77 mm is the wall length (see Figure 5a), and the Young modulus of the diagonal walls, E^d_{11} =3811 MPa, is that for the one-fabric-layer composite in Table 2. The result in Eq.(5) underestimates the effective values E_{xx} =93.09 MPa, E_{yy}=88.46 MPa that resulted from the homogenization analysis.

No analytical formulas were found in the bibliography that can be used or adapted to estimate G^*_{xy} and E^*_{zz}. Thus, a formula based on the relative transversal areas of the longitudinal and diagonal walls was developed to estimate E^*_{zz}. Consider to this purpose the unit element of the core depicted in Figure 5(b). The transversal areas of the diagonal and longitudinal walls are

$$A_d = 2l \cdot t \tag{6}$$

$$A_l = 2l \cdot \frac{t}{2}, \tag{7}$$

while the area for the unit element is

$$A_e = 2l \cdot [1 + \cos(60°) \cdot l \cdot \sin(60°)] = 3\frac{\sqrt{3}}{2}l^2. \tag{8}$$

Then, the equivalent Young modulus in the direction of the thickness can be estimated as follows

$$E_{zz}^{*} = \frac{A_d \cdot E_{11}^{d} + A_l \cdot E_{11}^{l}}{A_e} = 1102\ MPa, \tag{9}$$

where E_{11}^{d} and E_{11}^{l} are the Young modulus for the one- and two-fabric layer composites reported in Table 2. The E_{zz}^{*} estimated by Eq.(9) underestimates E_{zz}^{*}= 1225 MPa from the homogenization analysis by 10%.

For the verification of the out-of-plane elastic constant, we used the formulae due to Kelsey et al. [40], which specifies upper and lower bounds for the G_{xz} shear modulus. When specialized to regular hexagonal cores, the formulas due to Kelsey et al. [40] yield

$$\frac{\sqrt{3}\,t \cdot G_{12}}{3l} \leq G_{xz}^{*} \leq \frac{4\sqrt{3}t \cdot G_{12}}{9l} \tag{10}$$

$$134.81\ MPa \leq G_{xz}^{*} \leq 179.74\ MPa, \tag{11}$$

where the shear modulus G_{12}= 1226 MPa was taken as the average between the values measured for the one- and two-fabric-layer composites reported in Table 2. It is worth to note here that the almost identical shear response of the two composites (there is less than 2.5% difference in their shear modulus) allows using the formulae due to Kelsey et al. [40] for the present analysis. In what respects to the comparison of the results, it can be observed that the effective shear modulus of the core resulting from the homogenization analysis, G_{xz}= 170 MPa lies between the bounds of Eq. (10). Besides, $G_{xz}^{*}$was also computed using the formula proposed by Meraghni et al. [41], but it resulted in the same value that the upper bound due to Kelsey et al. [40] reported in Eq. (11).

Two formulas due to Kelsey et al. [40] and Meraghni et al. [41] were used to verify the G_{yz}. These are

$$G_{yz}^{*Meraghni} = \frac{G_{12} \cdot t\left(t+\sqrt{3}l\right)}{3l\left(t+\frac{\sqrt{3}}{2}l\right)} = 141.63\ MPa. \quad (12)$$

$$G_{yz}^{*Meraghni} = \frac{G_{12} \cdot t\left(t+\sqrt{3}l\right)}{3l\left(t+\frac{\sqrt{3}}{2}l\right)} = 141.63\ MPa. \quad (13)$$

The above results overestimate the effective value G_{yz} = 174 MPa in about 20%.

According to Gibson and Ashby [39] the regular hexagonal cores can be considered to have an isotropic elastic behavior in the *xy* plane. In this sense, it is interesting to observe that the results of the homogenization analysis provide evidence in that direction. We can see that computed values for the Young moduli E_{xx} and E_{yy} differ in less than 5.23%, while the difference between the shear moduli G_{xz} and G_{yz} is less than 2.5%.

Finally, the homogenized elasticity tensor was validated by comparison with the experimental results of the flexural modulus reported in Section 3.1.2. To this end, the bending test was modeled using three different approaches:

- *Full-detail model:* the geometry of the specimen was represented in full detail and shell elements (S4R) were used for its discretization, see Figure 14a. The elastic properties of the core walls were specified as C_1 or C_2, whether they corresponded to the one or two fabric-layer material, respectively. In order to study the effect of the element size on the value of the flexural modulus, a

convergence analysis was performed using element sizes ranging from 0.3 mm to 1 mm.

- *Solid model:* the specimen was represented as a prismatic body, which was discretized using hexahedral elements (C3D8R), see Figure 14b. The elastic properties were specified using the C_{eff}. The convergence analysis for the flexural modulus was performed using element sizes ranging from 0.7 mm to 1.5 mm.
- *Shell model:* the specimen was represented as a shell, which was discretized using S4R elements, see Figure 14c. The elastic properties were specified using the C_{eff}. The convergence analysis for the flexural modulus was performed using element sizes ranging from 0.2 mm to 1 mm.

The bending moments to the three models were applied by means of rigid cylinders, which interact to the specimens via friction-less contact boundary conditions, see Figure 14.

The results of the convergence analyses for the computation of the flexural modulus using the three models are plot in Figure 15. The modulus values computed via the extrapolation of the FEA results to zero-element size are compiled in Table 3. The shell-element model predicts a slightly higher modulus (around 3.5%) than the full-detail and the solid models. This result is coherent with the simpler and stiffer description of the problem associated to the shell model. At the same time, it can be observed that there is an excellent agreement between the experimental result and FE predictions (see Table 3). Maximum differences of 3.61% are for the full-detail and solid models, while for the shell model the difference is only 0.42%.

5. Conclusions

A novel honeycomb core made of a natural-fiber reinforced composite consisting of a vinylester matrix reinforced with jute fabric was introduced in this work. Six mm- and 10mm-cell honeycombs were manufactured by compression molding using two molds: a mold with fixed inserts and a mold that allows for lateral compression. The second method led to better results, as the lateral pressure allowed to obtain thinner walls and to better remove the excess of resin and to drag entrapped air bubbles.

The flatwise compression tests showed that the cores produced in this work do not exhibit the classical behavior observed for typical honeycombs, this is, they do not suffer of the unstable failure due to buckling of the cell walls, but a progressive damage due to typical fiber composite failure mechanisms, like yarn pull-out and fiber breaking. The large wall thickness relative to the cell size of the jute-vinylester cores, which inhibits buckling, and the heterogeneities in the composite material, which are preferential damage initiation sites, explain this behavior.

The jute-vinylester cores possess high compression strengths when compared to the commercially available cores: σ_c = 15.5 MPa for the 6mm-cell core and σ_c = 13.5 MPa for the 10mm-cell one. On the other hand, although the cores have relatively high densities, ρ =290 Kg/m^3 for the 6mm-cell core and ρ =157 Kg/m^3 for the 10mm-cell one, their specific compression strengths, σ_{cs}= 0.085 MPa/Kg and σ_{cs}= 0.05 MPa/Kg, are similar to those of commercially available cores.

The effective stiffness tensor of the 10-mm core was successfully computed via the experimental characterization of the elastic response of the composites and a finite element homogenization analysis. The results of the homogenization analysis are in good agreement with estimations of the effective engineering elastic constants computed via analytical formulas. Besides, very good agreement was found for a validation analysis where the flexural modulus of the core measured in experiments

was compared to the computed via finite element models with the homogenized stiffness tensor.

The results from this study suggest that jute-reinforced cores have the potential to be an alternative to standard cores in applications that sustain compressive static loads. Further research is needed to assess the performance of jute-reinforced cores when subjected to other loading configurations, like bending or dynamic loads.

Acknowledgements

The authors acknowledge the National Research Council (CONICET) and the National Agency for the Promotion of Science and Technology (ANPCYT) of the República Argentina (Grants PICT N°2472 and N°1154), and the National University of Mar del Plata for their financial support. The authors also wish to thank A.A. Ibarra Pino for kindly providing the Matlab code and his useful advice for the homogenization analysis.

REFERENCES

[1] Thomsen OT. Sandwich Materials for Wind Turbine Blades — Present and Future. Journal of Sandwich Structures and Materials. 2009;11:7-26.
[2] Hou S, Zhao S, Ren L, Han X, Li Q. Crashworthiness optimization of corrugated sandwich panels. Materials & Design. 2013;51:1071-84.
[3] Saha GC, Kalamkarov AL, Georgiades AV. Effective elastic characteristics of honeycomb sandwich composite shells made of generally orthotropic materials. Composites Part A: Applied Science and Manufacturing. 2007;38:1533-46.
[4] Li QM, Mines RAW, Birch RS. The crush behaviour of Rohacell-51WF structural foam. International Journal of Solids and Structures. 2000;37:6321-41.
[5] Da Silva A, Kyriakides S. Compressive response and failure of balsa wood. International Journal of Solids and Structures. 2007;44:8685-717.
[6] Lim C-H, Jeon I, Kang K-J. A new type of sandwich panel with periodic cellular metal cores and its mechanical performances. Materials & Design. 2009;30:3082-93.
[7] Sun Y, Gao L. Structural responses of all-composite improved-pyramidal truss sandwich cores. Materials & Design. 2013;43:50-8.
[8] Pflug J, Vangrimde B, Verpoest I, Bratfisch P, Vandepitte D. Continuously produced honeycomb cores. Advancing Materials in the Global Economy - Applications, Emerging Markets and Evolving Technologies. Long Beach, CA2003. p. 602-11.

[9] Pflug J, Vangrimde B, Verpoest I, Bratfisch P, Vandepitte D. Honeycomb Core Materials: New Concepts for Continuous Production. SAMPE Journal. 2003;39:22-30.
[10] Foo CC, Chai GB, Seah LK. Mechanical properties of Nomex material and Nomex honeycomb structure. Composite Structures. 2007;80:588-94.
[11] Pflug J, Verpoest I. Sandwich Materials Selection Charts. Journal of Sandwich Structures and Materials. 2006;8:407-21.
[12] Ji HS, Song W, Ma ZJ. Design, test and field application of a GFRP corrugated-core sandwich bridge. Engineering Structures. 2010;32:2814-24.
[13] Davalos JF, Chen A. Buckling Behavior of Honeycomb FRP Core with Partially Restrained Loaded Edges under Out-of-plane Compression. Journal of Composite Materials. 2005;39:1465-85.
[14] Santulli C, Sarasini F, Tirillò J, Valente T, Valente M, Caruso AP, et al. Mechanical behaviour of jute cloth/wool felts hybrid laminates. Materials & Design. 2013;50:309-21.
[15] Aziz SH, Ansell MP. The effect of alkalization and fibre alignment on the mechanical and thermal properties of kenaf and hemp bast fibre composites: Part 1 - polyester resin matrix. Composites Science and Technology. 2004;64:1219-30.
[16] Aziz SH, Ansell MP. The effect of alkalization and fibre alignment on the mechanical and thermal properties of kenaf and hemp bast fibre composites: part 2 - cashew nut shell liquid matrix. Composites Science and Technology. 2004;64:1231-8.
[17] Du Y, Yan N, Kortschot MT. Light-weight honeycomb core sandwich panels containing biofiber-reinforced thermoset polymer composite skins: Fabrication and evaluation. Composites Part B: Engineering. 2012;43:2875-82.
[18] Wambua P, Ivens J, Verpoest I. Natural fibres: can they replace glass in fibre reinforced plastics? Composites Science and Technology. 2003;63:1259-64.
[19] Azwa ZN, Yousif BF, Manalo AC, Karunasena W. A review on the degradability of polymeric composites based on natural fibres. Materials & Design. 2013;47:424-42.
[20] Singh B, Gupta M, Verma A. The durability of jute fibre-reinforced phenolic composites. Composites Science and Technology. 2000;60:581-9.
[21] Mwaikambo LY, Ansell MP. Chemical modification of hemp, sisal, jute, and kapok fibers by alkalization. Journal of Applied Polymer Science. 2002;84:2222-34.
[22] Dweib MA, Hu B, O'Donnell A, Shenton HW, Wool RP. All natural composite sandwich beams for structural applications. Composite Structures. 2004;63:147-57.
[23] Rao S, Jayaraman K, Bhattacharyya D. Natural fibre reinforced hollow core sandwich panels. 14th European Conference on Composite Materials. Budapest Hungary2010.
[24] Rao S, Jayaraman K, Bhattacharyya D. Short fibre reinforced cores and their sandwich panels: Processing and evaluation. Composites Part A: Applied Science and Manufacturing. 2011;42:1236-46.
[25] Petrone G, Rao S, De Rosa S, Mace BR, Franco F, Bhattacharyya D. Behaviour of fibre-reinforced honeycomb core under low velocity impact loading. Composite Structures. 2013;100:356-62.
[26] Petrone G, Rao S, De Rosa S, Mace BR, Franco F, Bhattacharyya D. Initial experimental investigations on natural fibre reinforced honeycomb core panels. Composites Part B: Engineering. 2013;55:400-6.
[27] Giglio M, Manes A, Gilioli A. Investigations on sandwich core properties through an experimental–numerical approach. Composites Part B: Engineering. 2012;43:361-74.
[28] Khan MK, Baig T, Mirza S. Experimental investigation of in-plane and out-of-plane crushing of aluminum honeycomb. Materials Science and Engineering: A. 2012;539:135-42.
[29] Zhang J, Ashby MF. The out-of-plane properties of honeycombs. International Journal of Mechanical Sciences. 1992;34:475-89.
[30] Eberl C, Thompson R, Bundschuh S. Multi-Scale Digital Image Correlation and Tracking with MATLAB. 2007.
[31] Bing P, Kemao Q, Huimin X, Anand A. Two-dimensional digital image correlation for in-plane displacement and strain measurement: a review. Measurement Science and Technology. 2009;20:062001.
[32] Hung P-C, Voloshin AS. In-plane strain measurement by digital image correlation. Journal of the Brazilian Society of Mechanical Sciences and Engineering. 2003;25:215-21.
[33] Pan B, Asundi A, Xie H, Gao J. Digital image correlation using iterative least squares and pointwise least squares for displacement field and strain field measurements. Optics and Lasers in Engineering. 2009;47:865-74.
[34] Simulia CDS. Abaqus Software Manual. 2009.
[35] Hashin Z. Analysis of Composite Materials---A Survey. Journal of Applied Mechanics. 1983;50:481-505.

[36] Ibarra Pino A. Estudio del comportamiento mecánico del hueso trabecular mediante técnicas de homogeneización. Phd Thesis, National University of Mar del plata. 2011.
[37] Barbero EJ. Finite Element Analysis of Composite Materials: CRC Press; 2008.
[38] Guedes J, Kikuchi N. Preprocessing and postprocessing for materials based on the homogenization method with adaptive finite element methods. Computer Methods in Applied Mechanics and Engineering. 1990;83:143-98.
[39] Gibson LJ, Ashby MF. Cellular Solids: Structure and Properties: Cambridge University Press; 1999.
[40] Kelsey S, Gellatly RA, Clark BW. The Shear Modulus of Foil Honeycomb Cores: A Theoretical and Experimental Investigation on Cores Used in Sandwich Construction. Aircraft Engineering and Aerospace Technology. 1958;30:294 - 302.
[41] Meraghni F, Desrumaux F, Benzeggagh ML. Mechanical behaviour of cellular core for structural sandwich panels. Composites Part A: Applied Science and Manufacturing. 1999;30:767-79.

FIGURE CAPTIONS

Figure 1: Mold with fixed inserts: a) bottom plate and inserts, b) pre-assembled honeycomb mold

Figure 2: Honeycomb core manufactured using the mold with the fixed inserts.

Figure 3: Mold with lateral compression: (a) Schematic of the manufacturing process; actual pictures of the (b) open and (c) closed mold.

Figure 4: Honeycomb manufactured using the lateral compression mold.

Figure 5: (a) Core coordinate system and (b) unit element and geometrical parameters

Figure 6: True stress vs strain curves resulting from the flatwise compression test.

Figure 7: Honeycomb core after compression test

Figure 8: SEM micrographs of the honeycomb cores failure mechanisms: (a) typical yarn pull-out, (b) closer view showing the fiber breakage and matrix plastic deformation.

Figure 9: Comparison between of the specific compression strengths of the jute/VE cores and those of the commercially available cores. Error bars in the jute/VE data indicate the dispersion of the experiments. Data obtained from product data sheet (*) and the **bibliography (**).

Figure 10: Specimens with a) their longitudinal and transversal directions coincident with the fabric orthotropic directions and b) rotated 45º.

Figure 11: a) Specimen for the uniaxial traction test with the speckle pattern for DIC measurements; b) Strain fields calculated by DIC for the load σ= 12 MPa.

Figure 12: Stress vs strain plots for the traction tests of the two-fabric-layer specimens with the load oriented 45º with respect to the fabric orthotropic directions.

Figure 13: FE model of the honeycomb unit cell: (a) model discretization and (b) deformed model for a shear load case.

Figure 14: Finite element models of the bending test: (a) full-detail model, (b) solid model, (c) shell model.

Figure 15: Results of the convergence analyses for the FEA analyses for computation of the flexural modulus of the 10mm-cell core.

Core type	Cell size c [mm]	Wall thickness t [mm]	Core height h [mm]	Density ρ [kg/m^3]	Compressive Strength σ_c [MPa]
Jute/VE honeycomb core	6	1.43	10	290	14.99
Jute/VE honeycomb core	10	1.11	10	157	13.48
Aluminium Plascore*	6.4	0.1	15.8	126	9.37
Stainless Steel Plascore*	9.5	n/a	12.7	92	2.41
Euro composite (special fiber)*	6.4	n/a	12.7	42	1.4
Hexcel HRH 10 Nomex**	4.7	0.15	19	32	0.9

* Data obtained from the product data sheet
** Data obtained from literature [23]

Table 1: Geometrical and compressive strength data of the honeycombs.

Material	Young´s Modulus, $E_{11} = E_{22}$ [MPa]	Poisson's ratio, ν_{12}	Shear modulus, G_{12} [MPa]
One-fabric-layer jute-vinylester composite	3811 ± 399	0,24 ± 0,03	1240 ±136
Two-fabric-layer jute-vinylester composite	7399 ± 302	0,26 ± 0,04	1211± 126

Table 2. Elastic properties of the jute-vinylester composites expressed in the fabric orthotropic directions.

	Flexural modulus [MPa]	Difference with respect to the experimental value
Experimental	115.48 ± 1.35	—
Full-detail model	111.31	3.61%
Solid model	111.55	3.40%
Shell model	114.99	0.42%

Table 3. Comparison between the flexural modulus measured in the experimental tests and those computed using finite element models with the homogenized elastic properties.

Figure 1

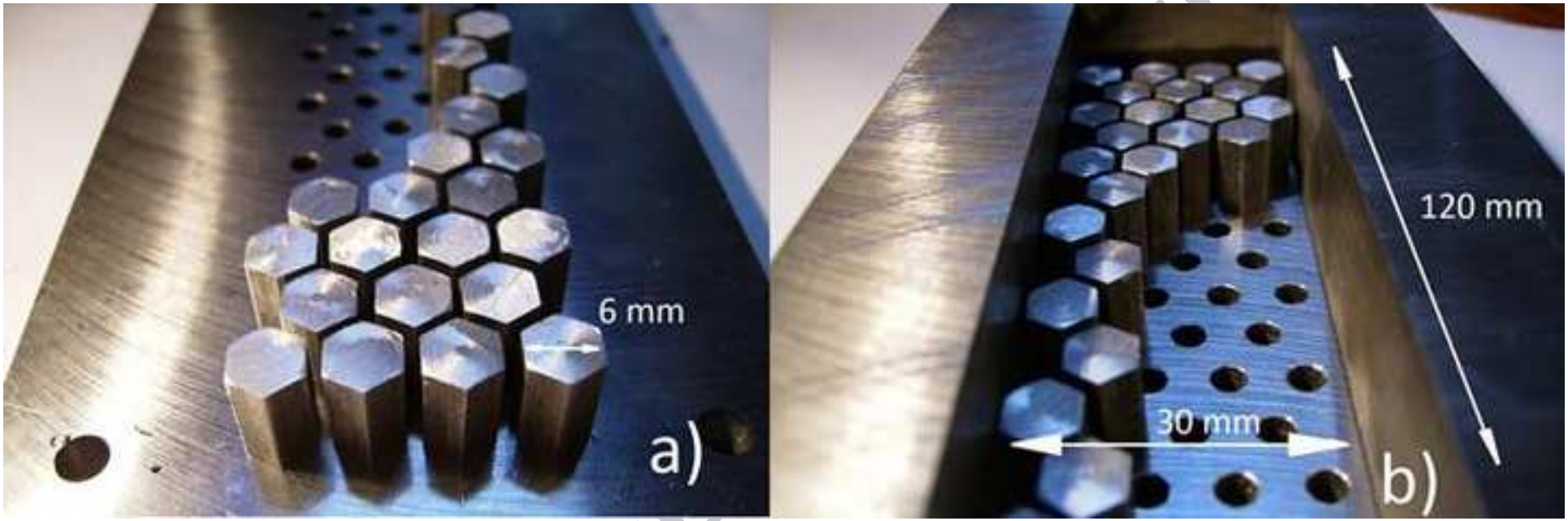

Figure 2

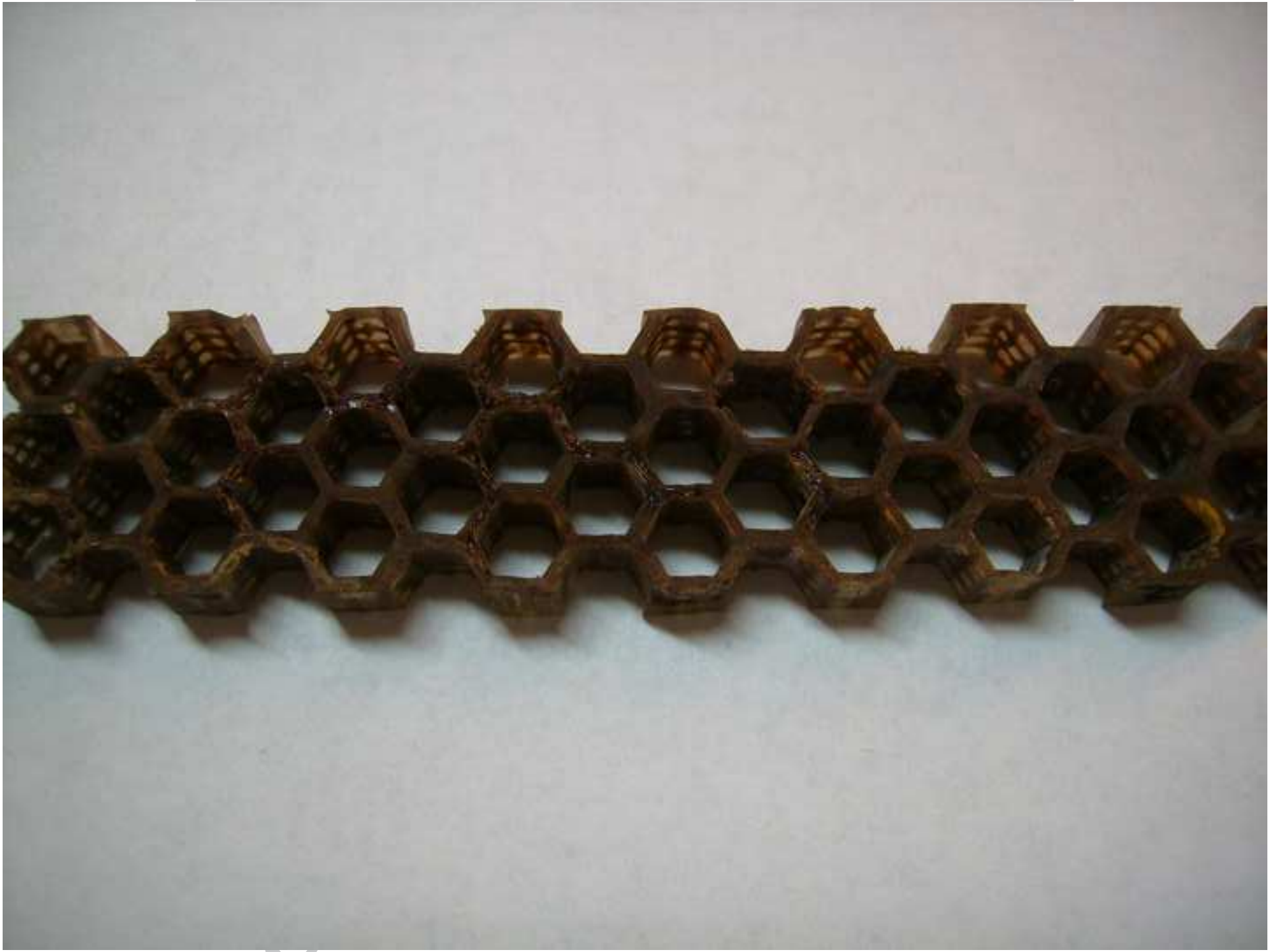

Figure 3

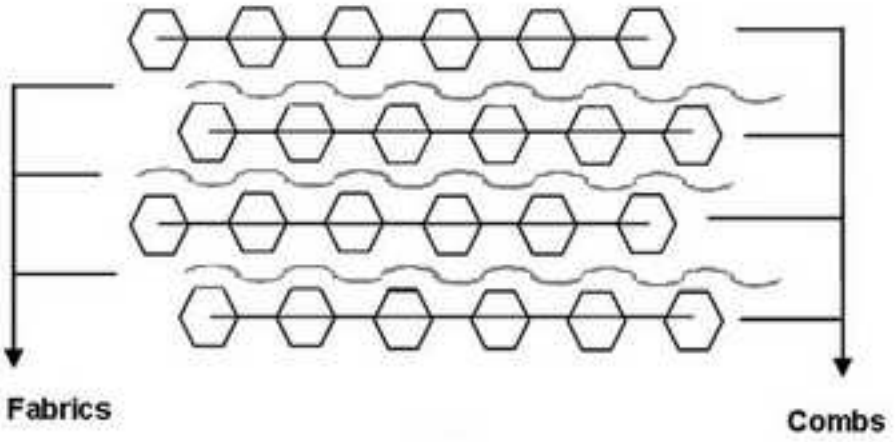

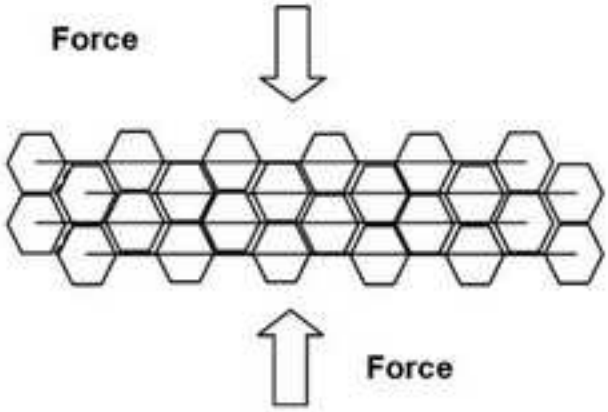

(a)

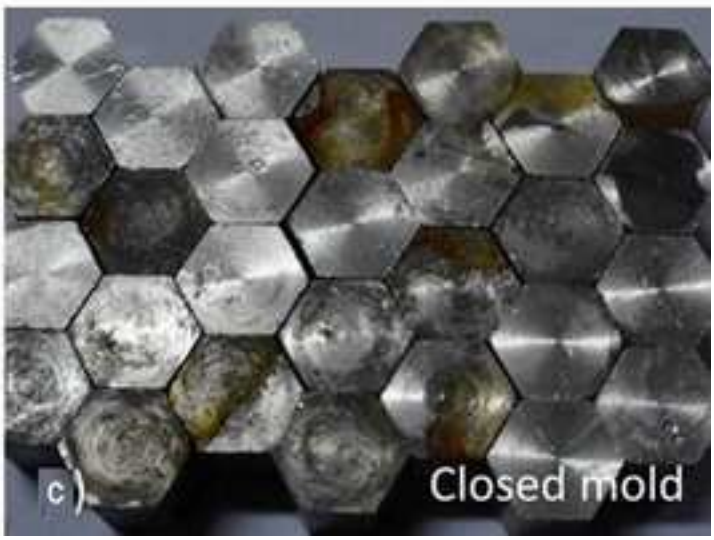

Figure 4

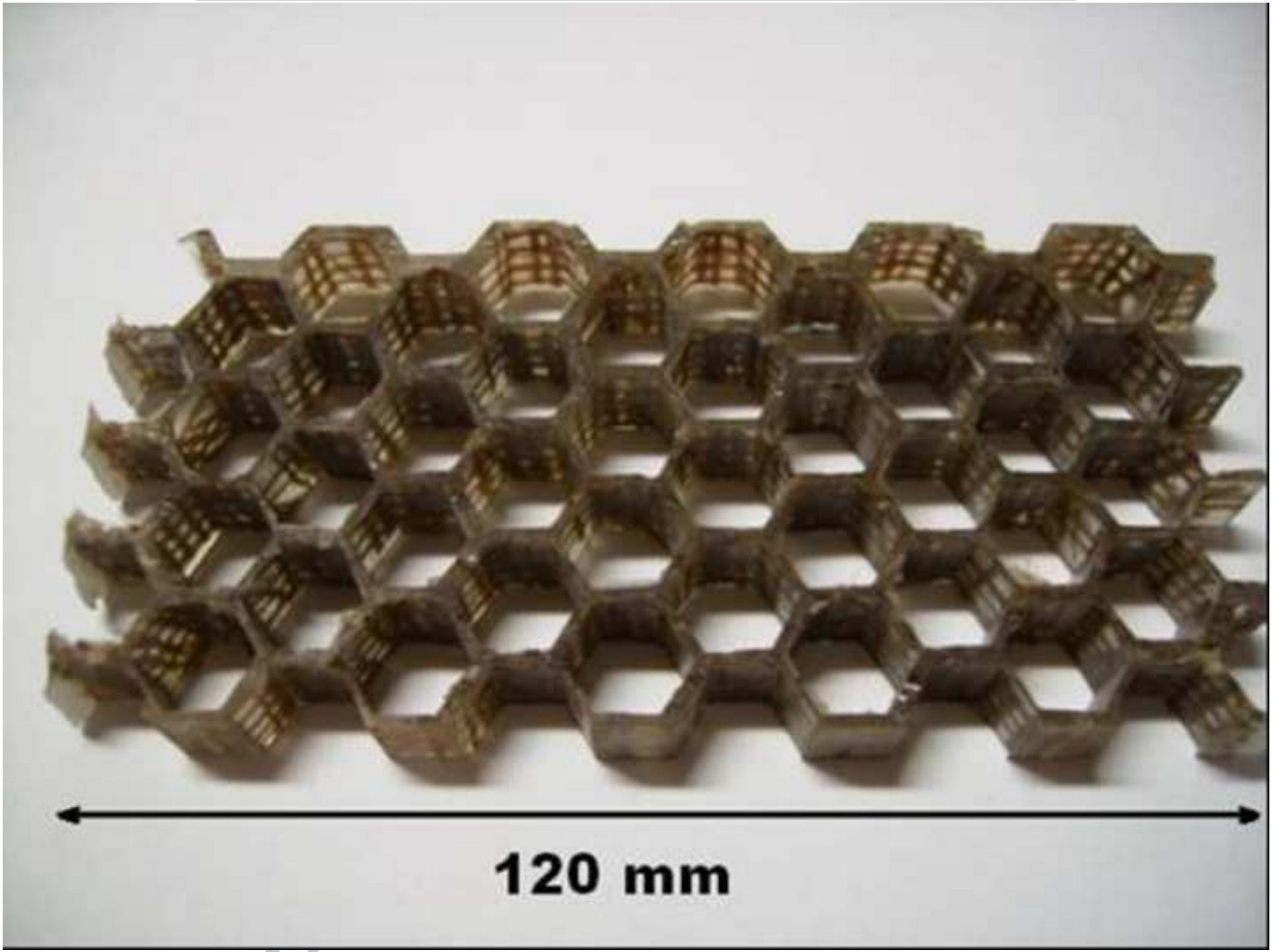

Figure 5

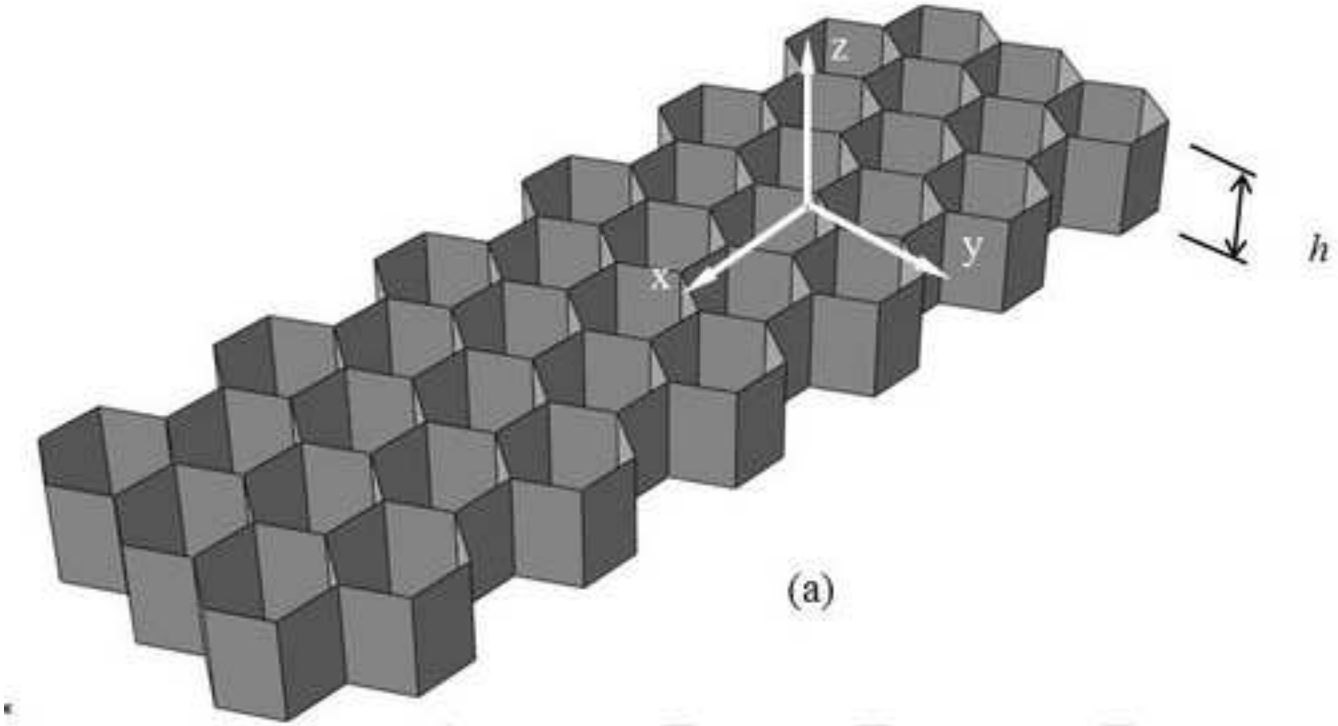

(a)

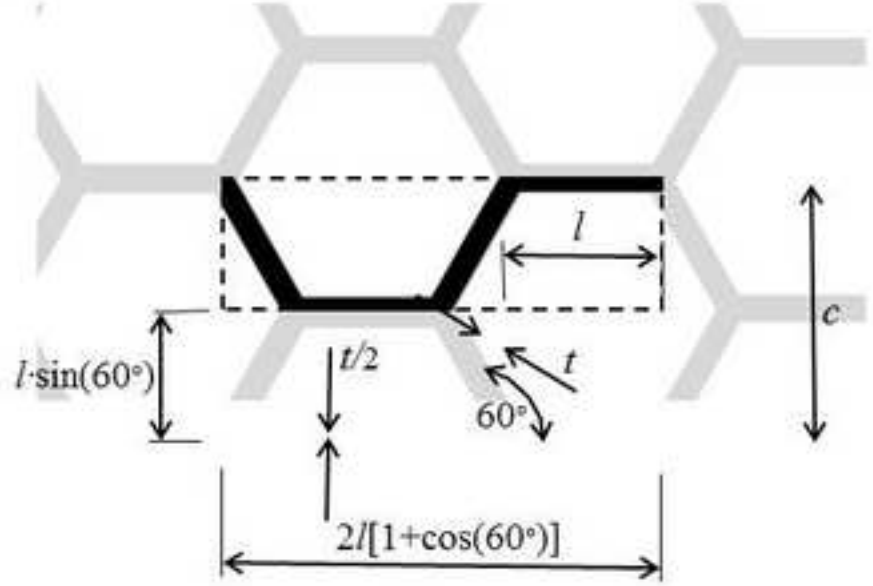

(b)

Figure 6

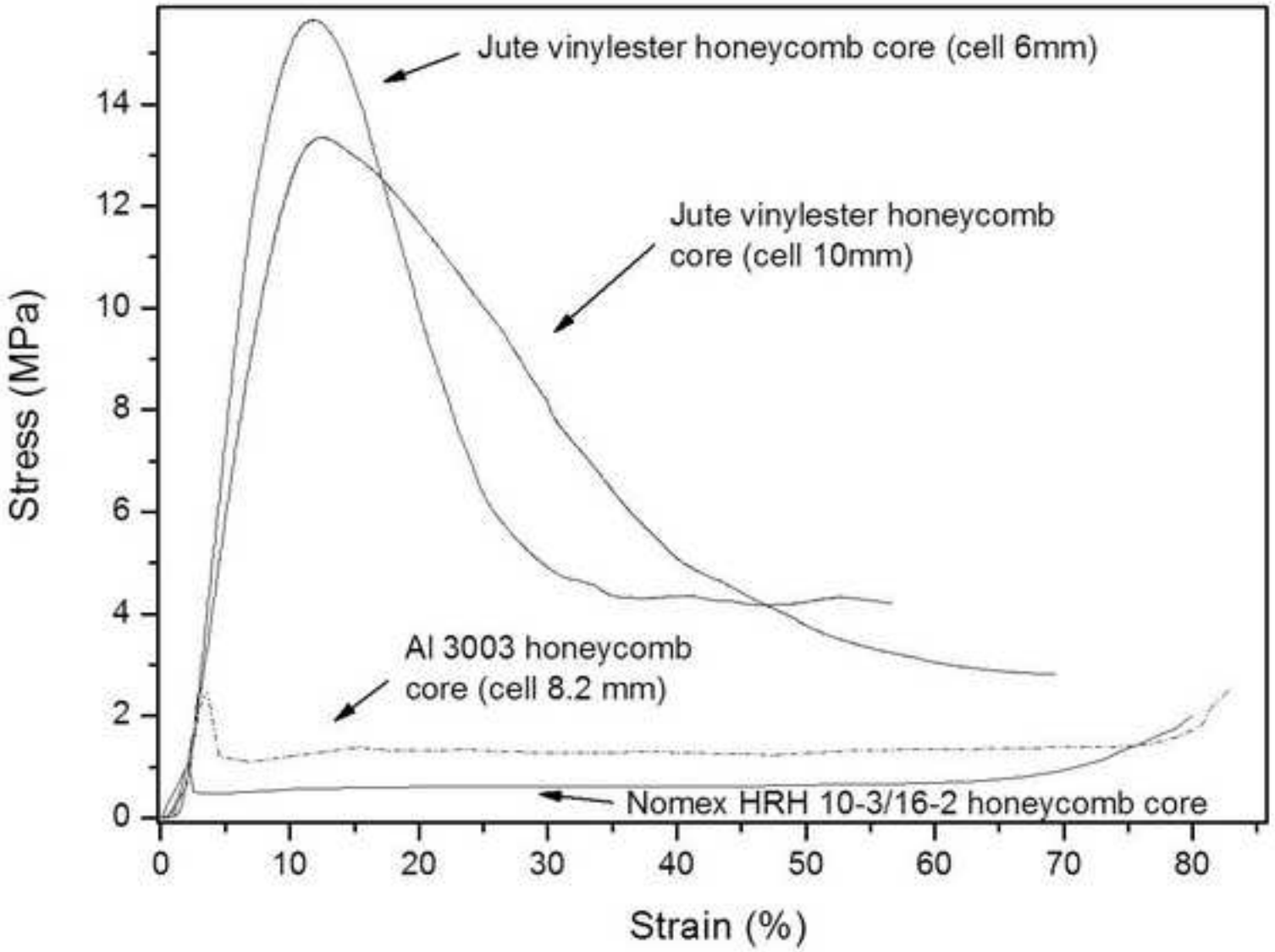

Figure 7

Figure 8

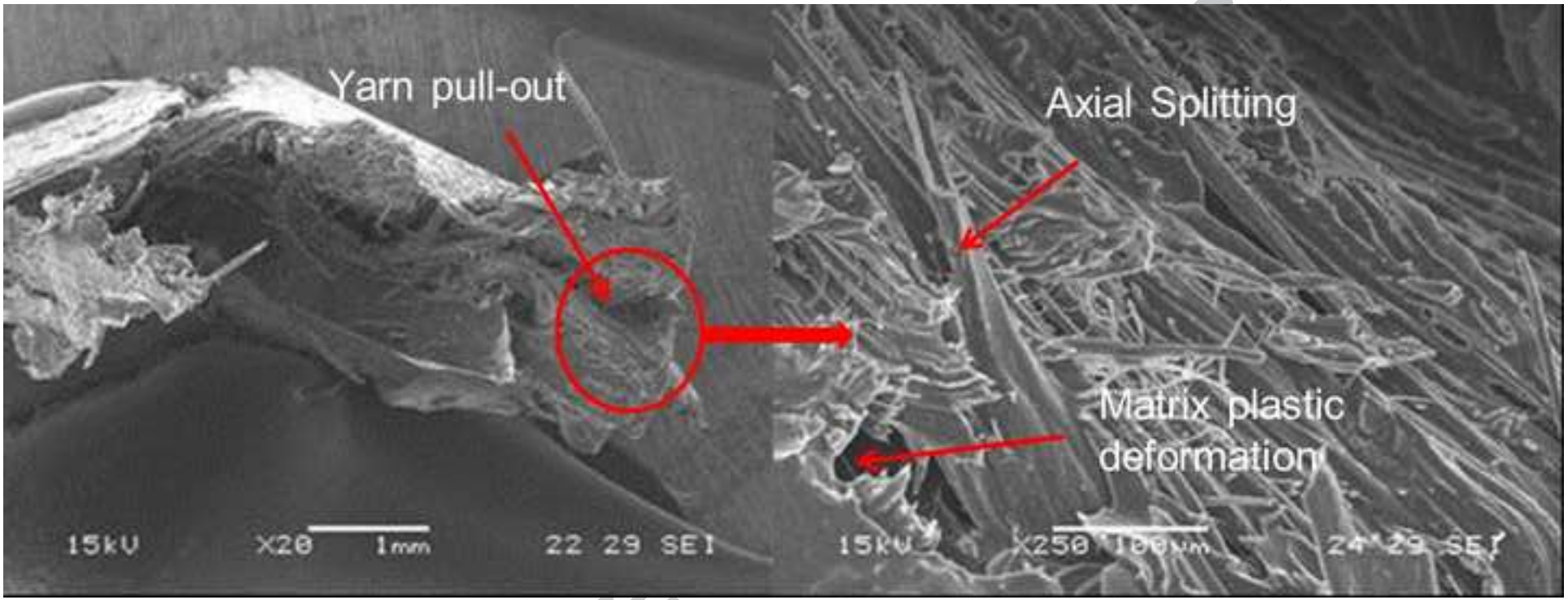

Figure 9

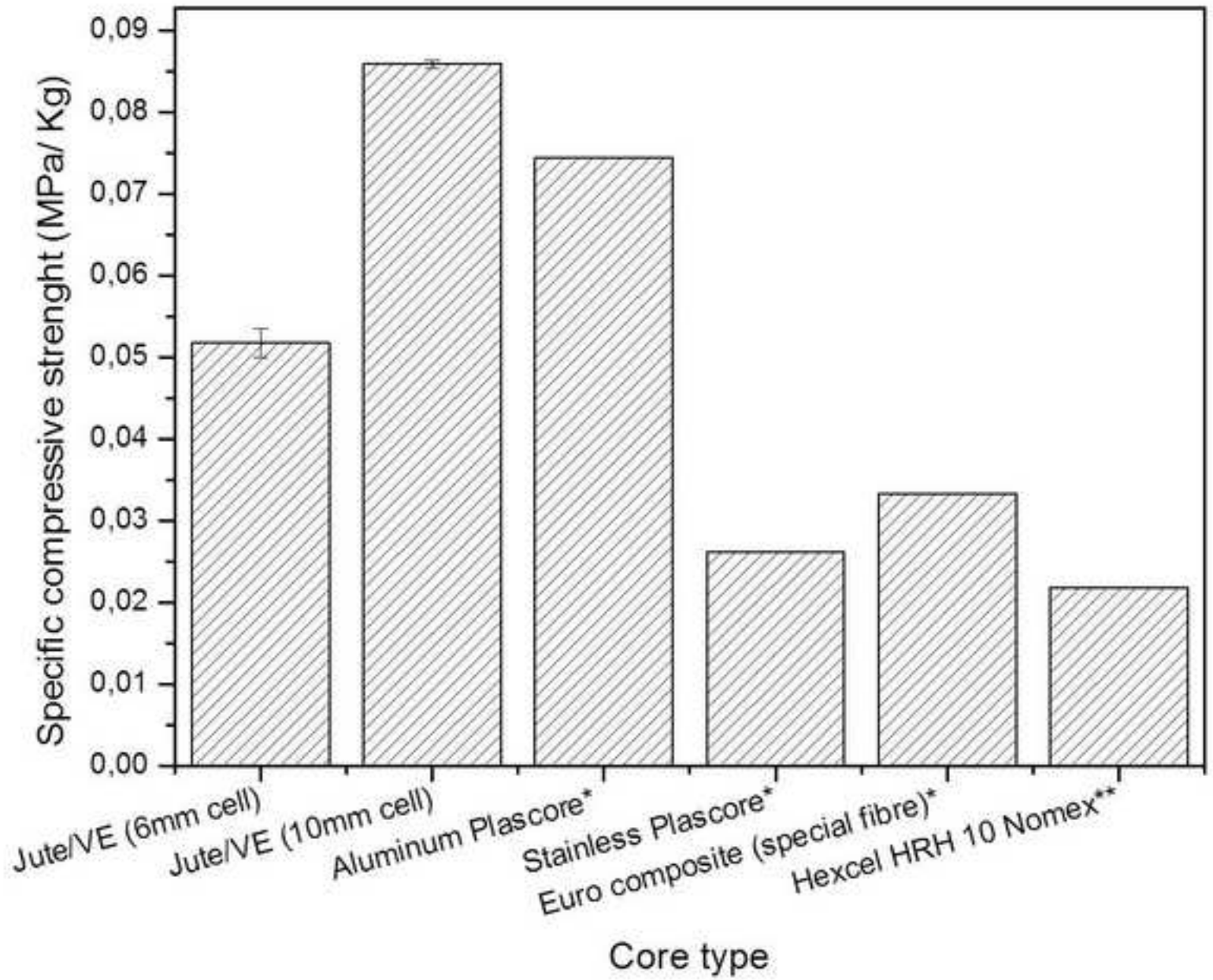

Figure 10

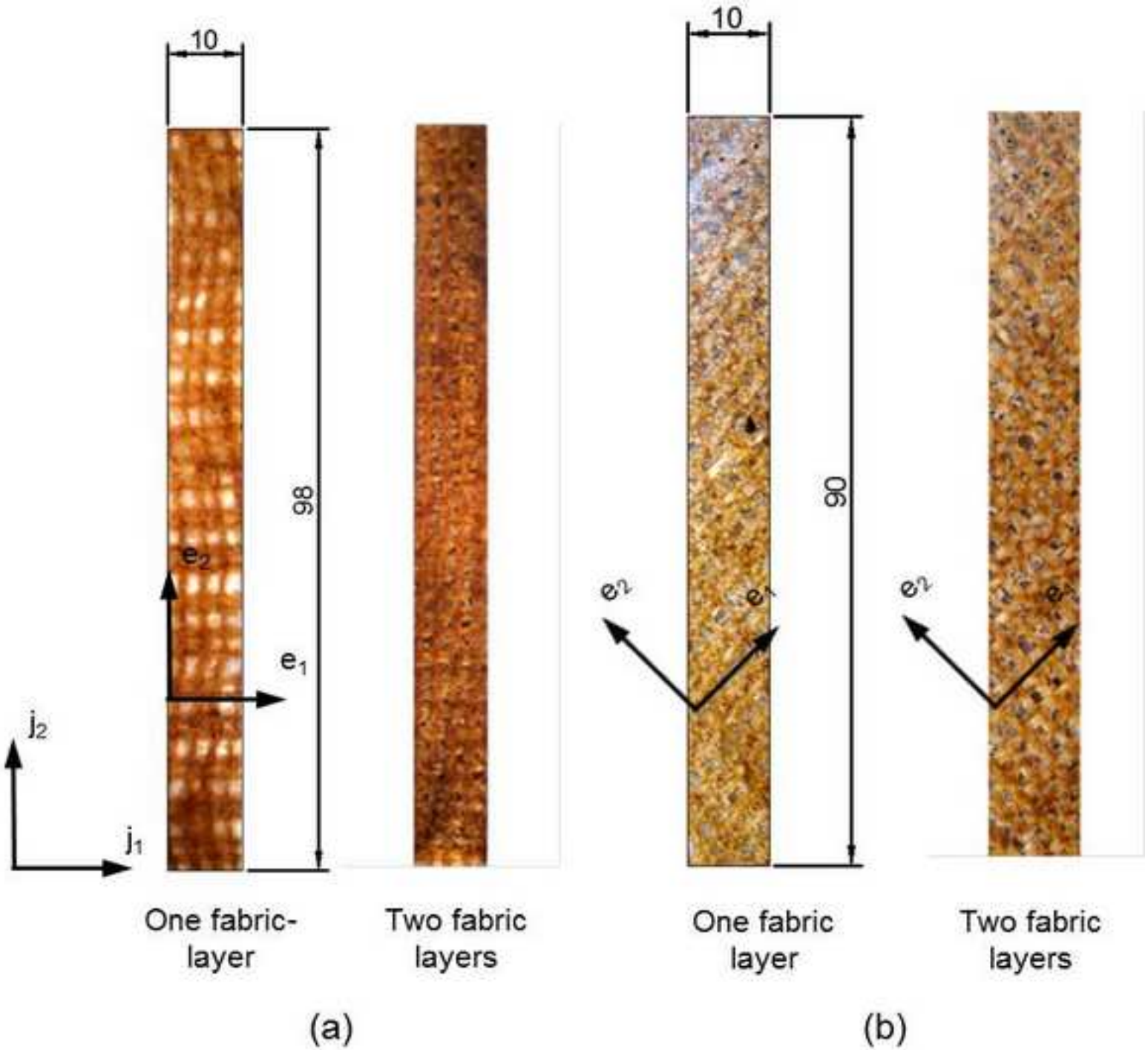

Figure 11

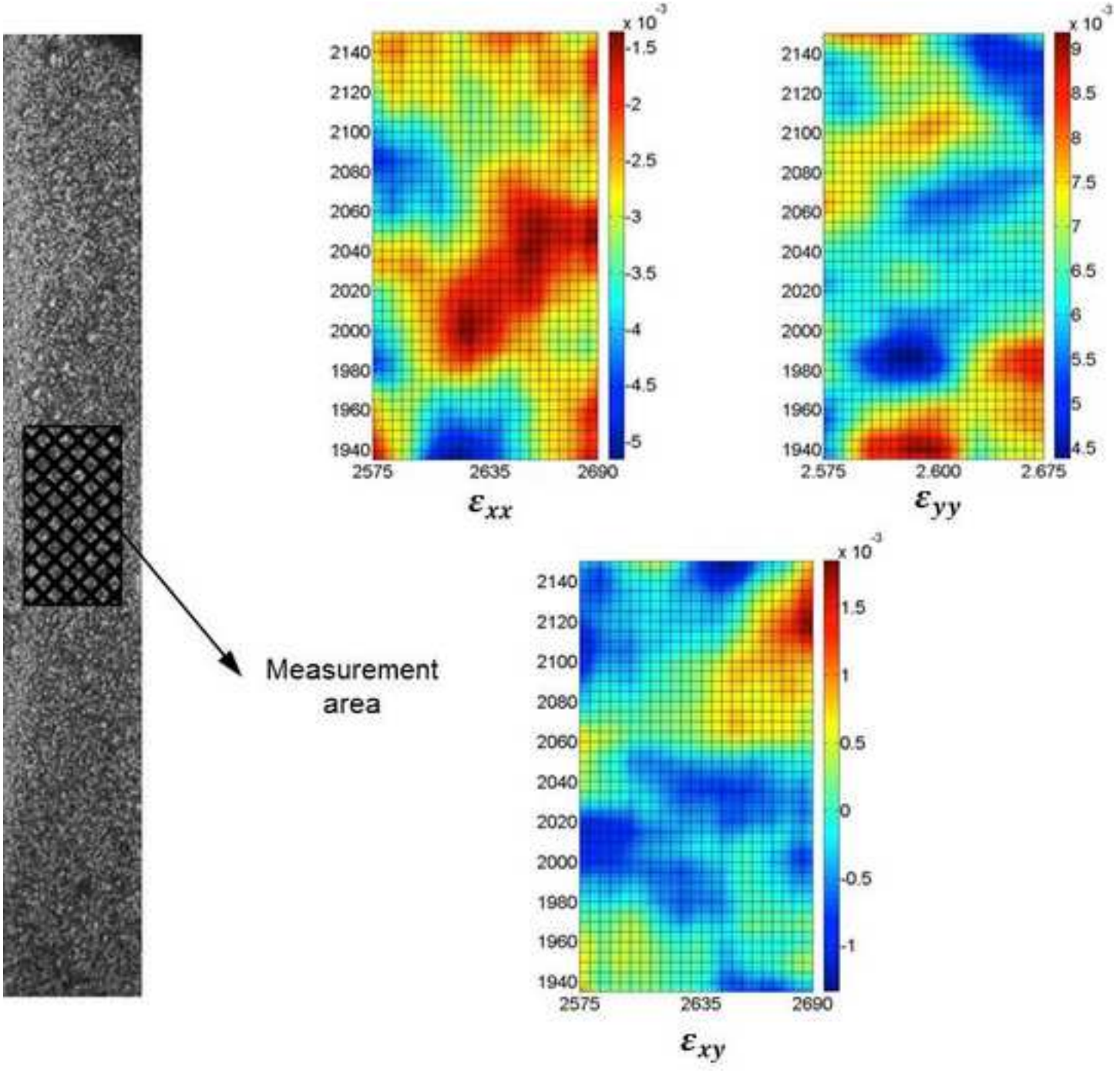

Figure 12

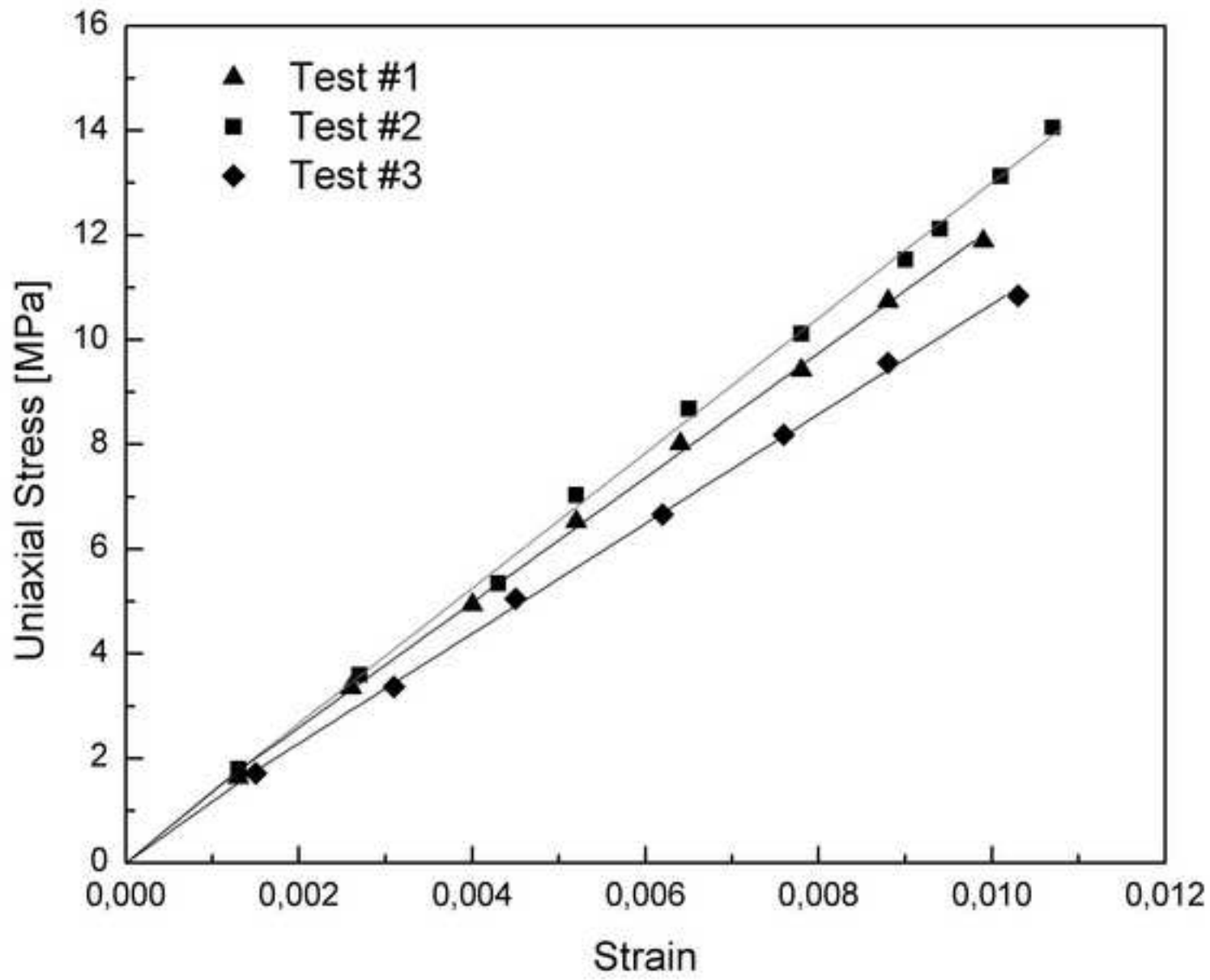

Figure 13

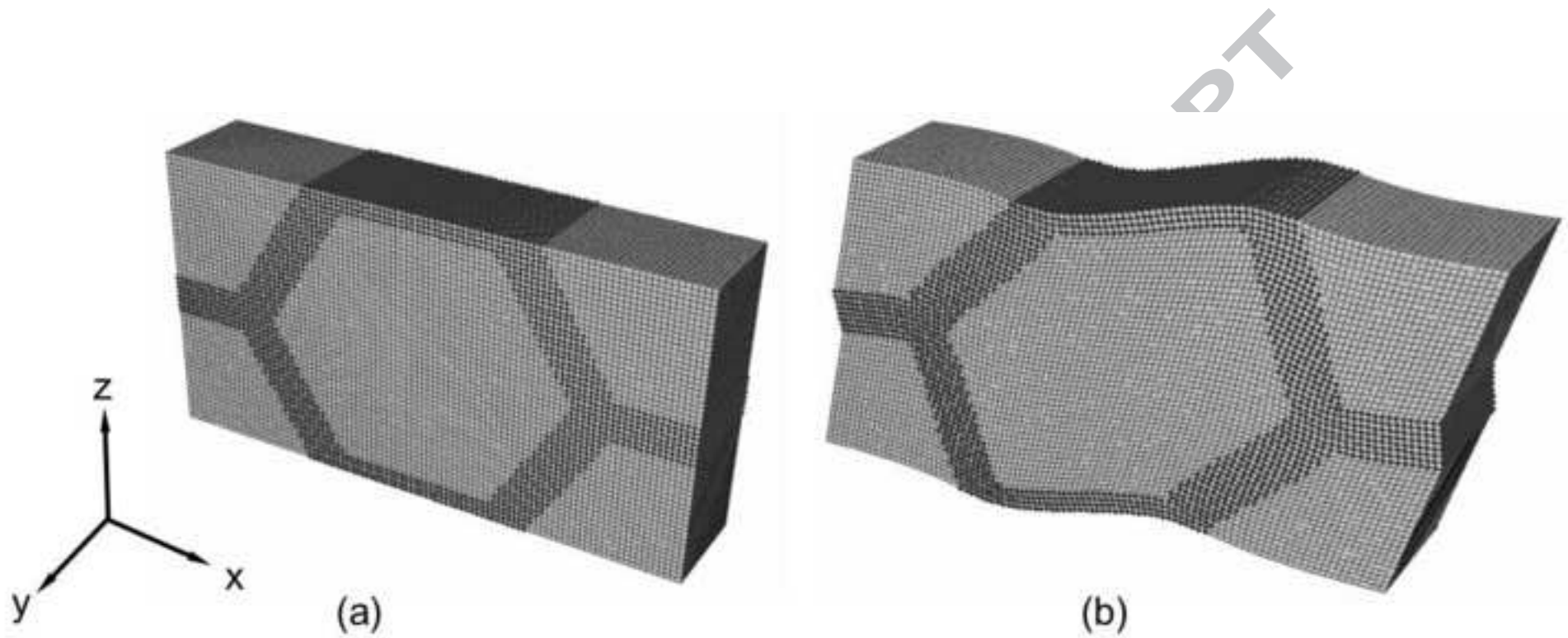

Figure 14

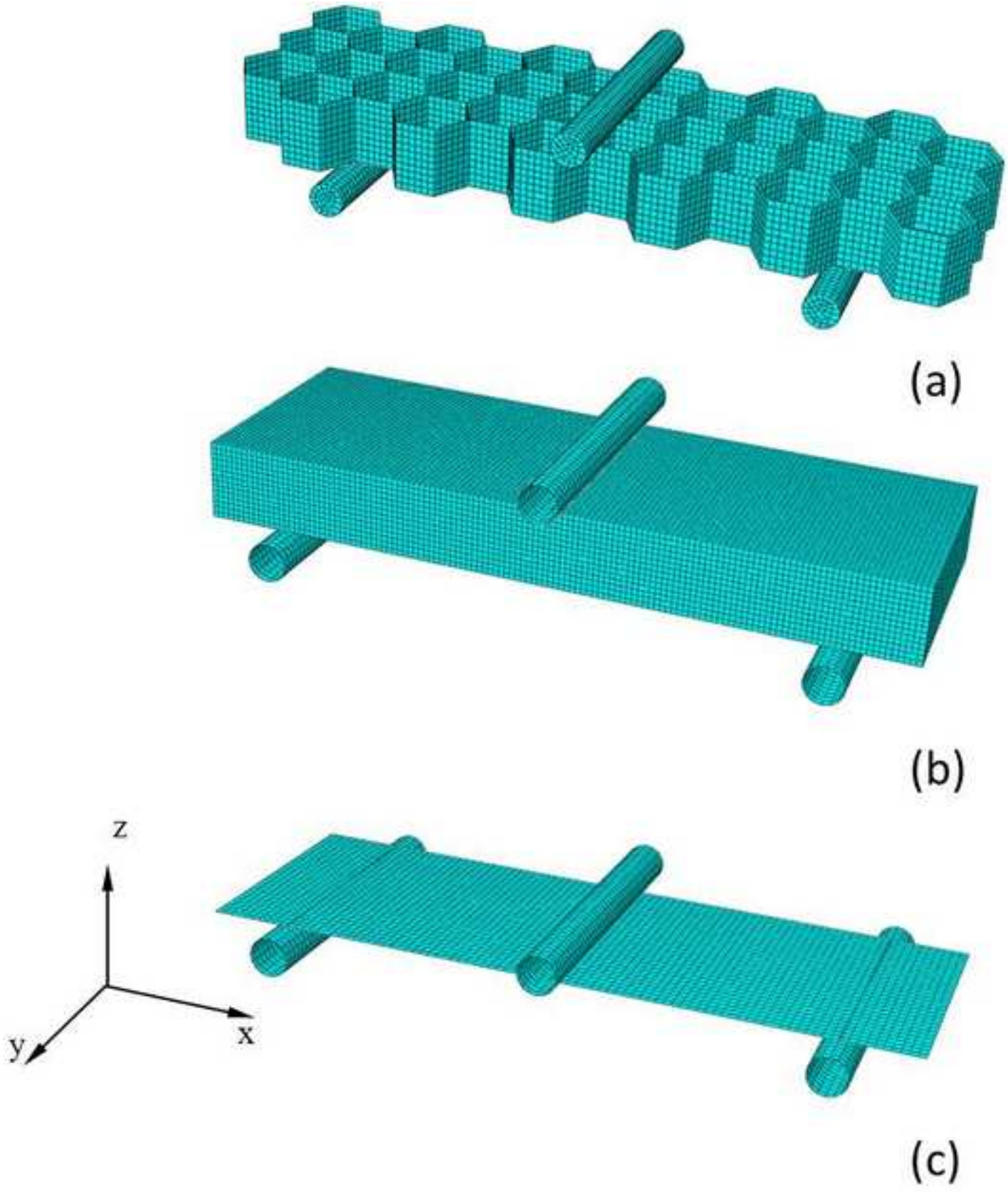

Figure 15

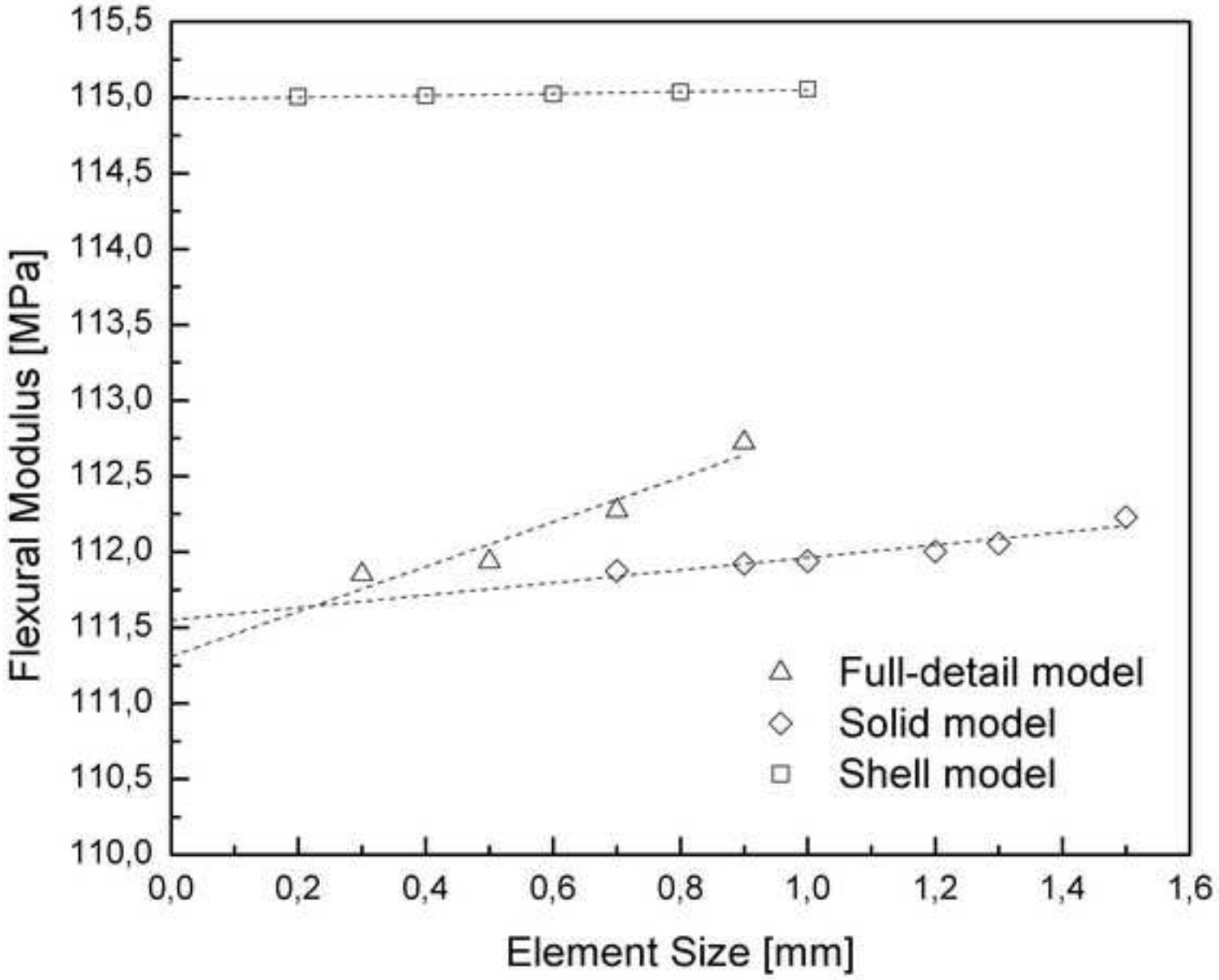

Highlights

- Honeycomb cores consisting of a vinylester matrix reinforced with jute fabrics were manufactured and tested.
- Experimental tests were conducted to characterize the elastic response of composite and core.
- The elastic properties were computed by homogenization analysis and finite element modeling.
- Fabricated cores can be a potential alternative to standard cores in several applications.
- Jute-vinylester cores have high density and compression strength in comparison to commercially available cores.